Meteoritics & Planetary Science 41, Nr 7, 989–1001 (2006)
Abstract available online at http://meteoritics.org

Fabric analysis of Allende matrix using EBSD

Lauren E. WATT[1*], Phil A. BLAND[1], Dave J. PRIOR[2], and Sara S. RUSSELL[3]

[1]IARC, Department of Earth Science and Engineering, Imperial College London, South Kensington Campus, London SW7 2AZ, UK
[2]Department of Earth and Ocean Sciences, University of Liverpool, 4 Brownlow Street, Liverpool L69 3GP, UK
[3]IARC, Department of Mineralogy, Natural History Museum, Cromwell Road, London SW7 5BD, UK
[*]Corresponding author. E-mail: lauren.watt@imperial.ac.uk

(Received 21 July 2005; revision accepted 25 March 2006)

Abstract–Fabric analysis of the interstitial matrix material in primitive meteorites offers a novel window on asteroid formation and evolution. Electron backscatter diffraction (EBSD) has allowed fabrics in these fine-grained materials to be visualized in detail for the first time. Our data reveal that Allende, a CV3 chondrite, possesses a uniform, planar, short-axis alignment fabric that is pervasive on a broad scale and is probably the result of deformational shortening related to impact or gravitational compaction. Interference between this matrix fabric and the larger, more rigid components, such as dark inclusions (DIs) and calcium-aluminium-rich inclusions (CAIs), has lead to the development of locally oriented and intensified matrix fabrics. In addition, DIs possess fabrics that are conformable with the broader matrix fabric. These results suggest that DIs were in situ prior to the deformational shortening event responsible for these fabrics, thus providing an argument against dark inclusions being fragments from another lithified part of the asteroid (Kojima and Tomeoka 1996; Fruland et al. 1978). Moreover, both DIs and Allende matrix are highly porous (~25%) (Corrigan et al. 1997). Mobilizing a highly porous DI during impact-induced brecciation without imposing a fabric and incorporating it into a highly porous matrix without significantly compacting these materials is improbable. We favor a model that involves Allende DIs, CAIs, and matrix accreting together and experiencing the same deformation events.

INTRODUCTION

Type 3 carbonaceous chondrites are among the most primitive examples of early solar system materials available to us. They contain components that formed prior to the accretion of their parent asteroid and thus provide unique insights into the earliest history of the solar nebula and the subsequent formation of our planetary system (Brearley and Jones 1998). These meteorites contain a variety of different components, including chondrules, calcium-aluminium-rich inclusions (CAIs), dark inclusions (DIs), and abundant fine-grained (<5 μm) matrix material, which is interstitial to these larger components.

Fabric analysis has been used by geologists for decades to provide insights into the processes that have acted on rocks during and after their formation. Understanding these processes has helped geologists answer fundamental questions about how these rocks formed and were subsequently deformed. The application of fabric analysis to meteorites can help us determine how the different components came together, what the relationship is between components, and what processes have acted on them following accretion. Fabric analysis is therefore of key importance to understanding the record of early solar system processes contained in meteorites. Previously, fabric analysis of these meteorites has been confined to studies of bulk meteorite fabrics using X-ray pole figure goniometry (Fujimura et al. 1983), magnetic susceptibility (Sneyd et al. 1988), natural remnant magnetization (Morden and Collinson 1992), and qualitative observations of the large-scale (>100 μm) components such as flattened chondrules (Tomeoka et al. 1999). The fine-grained matrix material has largely been exempt from fabric analysis because it is beyond the resolution of most traditional fabric analytical techniques. However, matrix typically constitutes ~30–50 vol% (Brearley and Jones 1998) in type 3 carbonaceous chondrites (CV3s and CO3s) and its interstitial nature means that detailed crystallographic and fabric analysis of this material would be very helpful in understanding asteroid formation and evolution.

This work uses electron backscatter diffraction (EBSD) to analyze the matrix of Allende, a type 3 carbonaceous

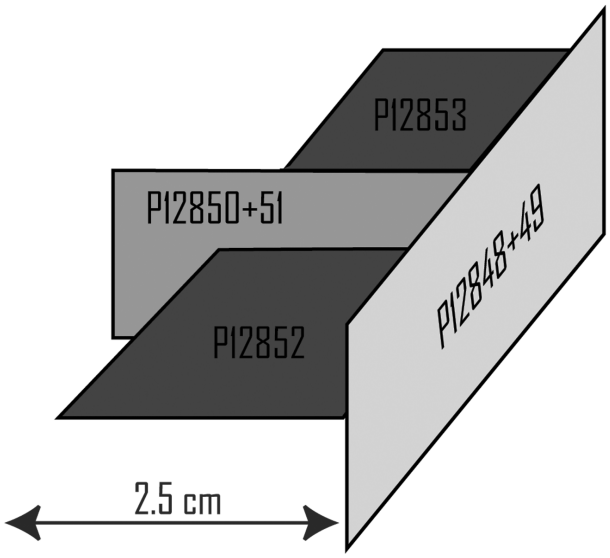

Fig. 1. A schematic diagram showing a 3-D configuration of thick sections P12848–P12853. Note that sections P12848 and 49 and sections P12850 and 51 were cut parallel to each other.

chondrite of the Vigarano group (CV3). Matrix material in CV3 chondrites is a porous aggregate (average porosity ~10%) of fine-grained minerals (average = ~5 μm) (Scott et al. 1988), which occur as rims on chondrules and other components as well as interstitial material, which tends to be coarser grained (Scott and Krot 2003). Fayalitic olivine is the major component of the CV3 matrix (>80 vol%) (Weisberg and Prinz 1998) and occurs as two distinct morphological types (Brearley and Jones 1998):

1. Elongate, platy, tabular, and lath-shaped euhedral crystals; these can reach up to 20 μm in length and 1–3 μm in thickness.
2. Subhedral to irregularly shaped grains; these are generally much finer grained (<100 nm–3 μm) and occur in the interstices between the elongate olivines.

The abundance of these different forms varies widely among the CV3 chondrites. In the case of Allende, the elongate, euhedral crystals are particularly abundant, giving rise to a coarser average grain size than many other CV3s (Krot et al. 1995). CV3 chondrites have an average matrix olivine composition of ~Fa_{50} (Scott et al. 1988). However, matrix olivine compositions can be highly variable within individual CV3 chondrites, and from one CV3 chondrite to another. Allende has a well-defined range of $Fa_{45–56}$ (Peck 1984).

Clinopyroxene is the second most abundant phase in CV3 matrix material, with its composition ranging from hedenbergite to diopside (Scott et al. 1988). A variety of accessory phases are also present in varying amounts, including feldspathoids, phyllosilicates, oxides, and sulfides (Scott et al. 1988). The origin of the major silicate phases in CV3 chondrites is a subject of extensive debate, with models of both nebular and asteroidal origins being proposed. We believe EBSD analysis of CV3 matrix may help untangle this problem.

Electron backscatter diffraction (EBSD) is a scanning electron microscope (SEM) technique that permits the measurements of the full crystallographic orientation of any point (Prior et al. 1999). Backscattered electrons (BSEs) that escape from the specimen will form a diffraction pattern that can be imaged on a phosphor screen. Crystallographic orientations are obtained by automatically indexing these diffraction patterns (Bestmann and Prior 2003) and analysis of these data enables us to quantify fabrics that may be present. This technique has been applied to a wide range of terrestrial rocks. However, due to recent advances in microscopy, it has become possible to analyze the full crystallographic orientation of the fine-grained (submicron) matrix material in chondrites using this technique, allowing fabrics in these materials to be visualized in detail for the first time (Bland et al. 2003). This technique was first applied to fayalitic olivines in chondritic meteorite by Bland et al. (2003) and P. A. Bland (personal communication, 2003). Their work revealed that in chondrule rims in Allende, a CV3 carbonaceous chondrite, there is a well developed, short <a>-axis alignment fabric (fiber fabric), where the <a>-axis of the matrix olivines remains perpendicular to the chondrule margin around the entire perimeter of the chondrule. Thus, platy olivine grains, with a short <a>-axis, appear to "tile" chondrules. This study follows on from Bland et al.'s (2003) work and focuses on using EBSD to identify and analyze fabrics within the fayalitic component (~80 vol%) of Allende matrix, and elucidate the relationship between matrix and the larger components of this meteorite.

TERMINOLOGY

Many terms have been used in the geological, metallurgical, and materials science literatures to describe the analysis of "lattice preferred orientations" (LPO, the preferred orientation of crystallographic axes or planes). In the geological literature, "crystallographic preferred orientation" (CPO) is used synonymously with LPO, while in the materials science and metallurgy literature, "texture" or "macrotexture" is used to describe LPO. In geological studies, "fabric" is used to refer to material anisotropies in the broadest sense, including LPOs. Since the term "fabric" has already been applied to meteorite studies, we will use it here to be synonymous with LPO.

SAMPLES AND TECHNIQUE

To aid the identification of any fabrics present in Allende matrix, we analyzed six thick sections (P12848–P12853; ~150 μm in thickness) cut in a 3-D configuration (Fig. 1). These sections contain abundant chondrules and CAIs, which also permitted the study of the relationship between the

matrix and these components. Additionally, we analyzed five thin sections (~30 μm) of Allende, which contained type B dark inclusions, in order to investigate the relationship between matrix and DIs. The relative spatial relationship between these five sections is unknown.

Backscattered electron (BSE) mosaics were obtained using an LEO 1455VP for each of these polished sections and were used to determine sites of interest for EBSD analysis.

To obtain full crystallographic orientation data for these sites of interest, samples were analyzed in a CamScan X500 crystal probe fitted with a thermionic field emission gun (Bestmann and Prior 2003) and were mapped by beam movement on a grid with a fixed step of 0.2 μm to ensure that each (sub)grain contained several measurement points. The EBSD pattern from each point was indexed using the program CHANNEL 5.1 from HKL, enabling the construction of pattern quality maps (Fig. 2), orientation maps and equal area, pole figure plots of crystallographic orientations for a given area (Fig. 3).

In pattern quality (or band contrast) maps, gray shades relate to a quantitative image analysis parameter of the EBSD pattern, with dark pixels indicating poor pattern quality and bright pixels indicating good pattern quality (Fig. 2). They are a useful tool to verify the reliability of the orientation maps (Bestmann and Prior 2003). For orientation maps, the color of every pixel is generated by superposition of three color channels (red, green, and blue), which are assigned the values of the three Euler angles (φ1, Φ, φ2) of each measured point. Changes in color represent changes in grain orientation, however, because of the way that Euler angles are defined, sudden changes of color can occur that do not correspond to large changes in orientation (Bestmann and Prior 2003). When analyzing crystallographic data for olivine, due to its orthorhombic crystal structure, there are three crystal directions of interest, the <100>, <010>, and <001> directions. Each direction is plotted as a point in its own pole figure plot (Fig. 3). These directions can be thought of as crystallographic axes; for example, a data point on pole figure <100> represents the 3-D orientation of the <a>-axis for that crystal.

Once an area is mapped, the data are processed to ensure there is no bias toward larger grains and that misindexed points are not included in the analysis. Because the step size (0.2 μm) is much smaller than the grain size (average ~5 μm), nonsystematic errors can be identified as individual data points that are different from all surrounding data points. An automatic filter removes such points. Data points that are incorrectly indexed in a systematic manner are more problematic (Bestmann and Prior 2003). These occur where the stronger diffraction bands in two different patterns are sufficiently similar to be indistinguishable by the indexing software (Bestmann and Prior 2003). However, these points are usually significantly smaller than the average grain size and are removed by filtering out the smallest data points.

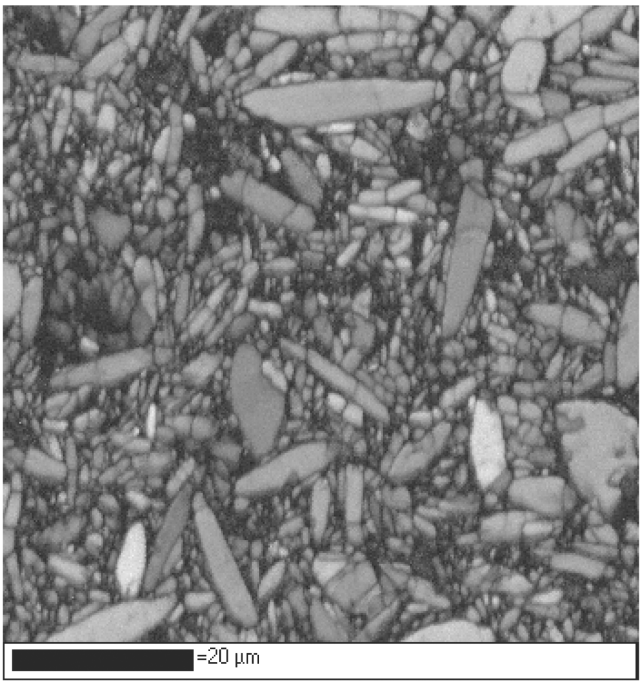

Fig. 2. A grayscale pattern quality map of Allende matrix. Bright pixels = high image quality; dark pixels = low image quality.

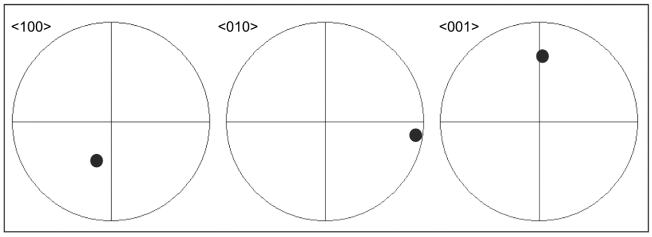

Fig. 3. An equal area, lower hemisphere pole figure plot for a single olivine crystal. Olivine is orthorhombic, with 3 principle crystallographic direction (<100>, <010>, and <001>), each represented by its own equal area, lower hemisphere pole figure plot.

Grains smaller than approximately 4× the step size are approaching the spatial resolution for EBSD and become unreliable. Since the data are mapped at a 0.2 μm step-size, grains smaller than 0.8 μm must be disregarded. This cutoff is also adequate for removing the systematic misindexed points. Larger grains will contain more data points than smaller grains, thus, a single large crystal can impose a dominant signal on any fabric orientation plot. To ensure there is no bias toward the larger grains, the data set is further reduced to one point per grain. Once the data are processed, each point, representing a single grain, is plotted on an equal area, lower hemisphere pole figure plot (Figs. 3 and 4b).

Data are contoured, using a counting cone of 15 degrees (Fig 4c), and clustering of the points reveal fabrics that may be present. There are three basic patterns generally observed:

a. Random: No clustering of axes.

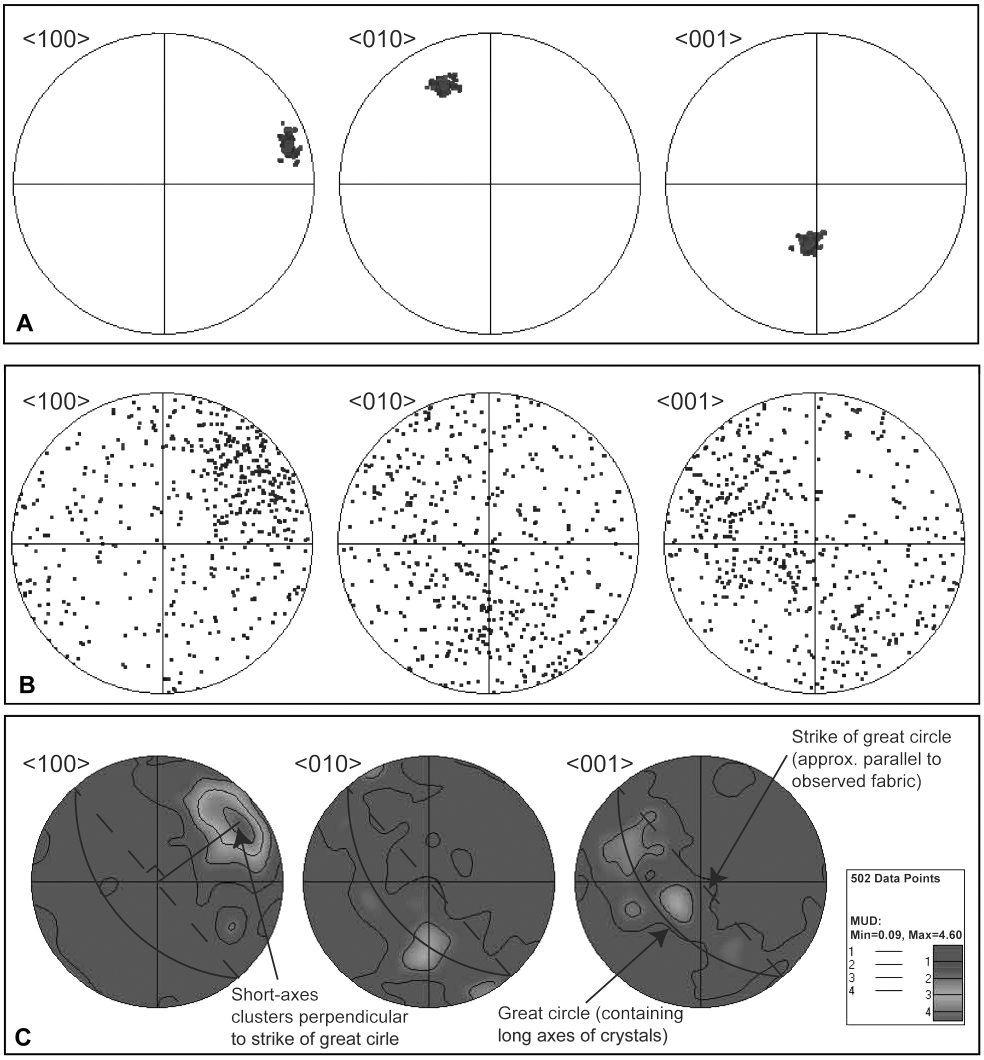

Fig. 4. Equal area, lower hemisphere pole figure plots describing general fabrics observed using EBSD. a) A single crystal fabric where all data points cluster around the orientation of a single crystal. b) A pole figure displaying point data (one point per grain), representing short-axis alignment fabric. c) Contoured point data (Fig. 4b), highlighting short-axis alignment fabric, with two axes spread around the same great circle (<010> and <001> directions), the strike of which is parallel to the observed fabric, and the short axes plotting perpendicular to the strike of this great circle (<a>-axis; <100> direction), with maximum intensity 4.6 MUD.

b. Single crystal fabric (Fig. 4a): All the grains have approximately the same orientation and therefore cluster around the orientation of a single grain. All three principal directions are clustered.
c. Short-axis alignment fabric/fiber fabric (Figs. 4b and 4c): Grains appear random in plan-view (if the section is parallel to the fabric), but stacked like tiles in cross section. Two of the principle directions, corresponding to the long axes of the crystals, spread around the same great circle (e.g., <010> and <001>) (Fig. 4c), whose strike is approximately parallel to the fabric observed. The other direction (e.g., <100>) (Fig 4c) clusters perpendicular to the strike of this great circle, corresponding to the short axis of the crystals that form the fabric (i.e., the <a>-axis is short in this example).

Note: The fabric in Figs. 4b and 4c is not in not parallel to the section.

For EBSD, the statistical description of the intensity of a fabric is known as the multiple of uniform density (MUD) and is quantified using the maximum intensity of the contoured pole figures (e.g., Fig. 4c). A maximum MUD of 1 represents a random fabric, i.e., if all of the data points are plotted they would be distributed evenly across the projection. A maximum MUD significantly greater than 1 is indicative of a fabric. However, the fabric intensity is related to the sample size; in small data sets, it is possible to get an apparent increase in fabric intensity. Therefore, in order to compare fabric intensities between different sites of interest, we keep the sample size reasonably consistent. A minimum of ~100–150 grain measurements are required to obtain a

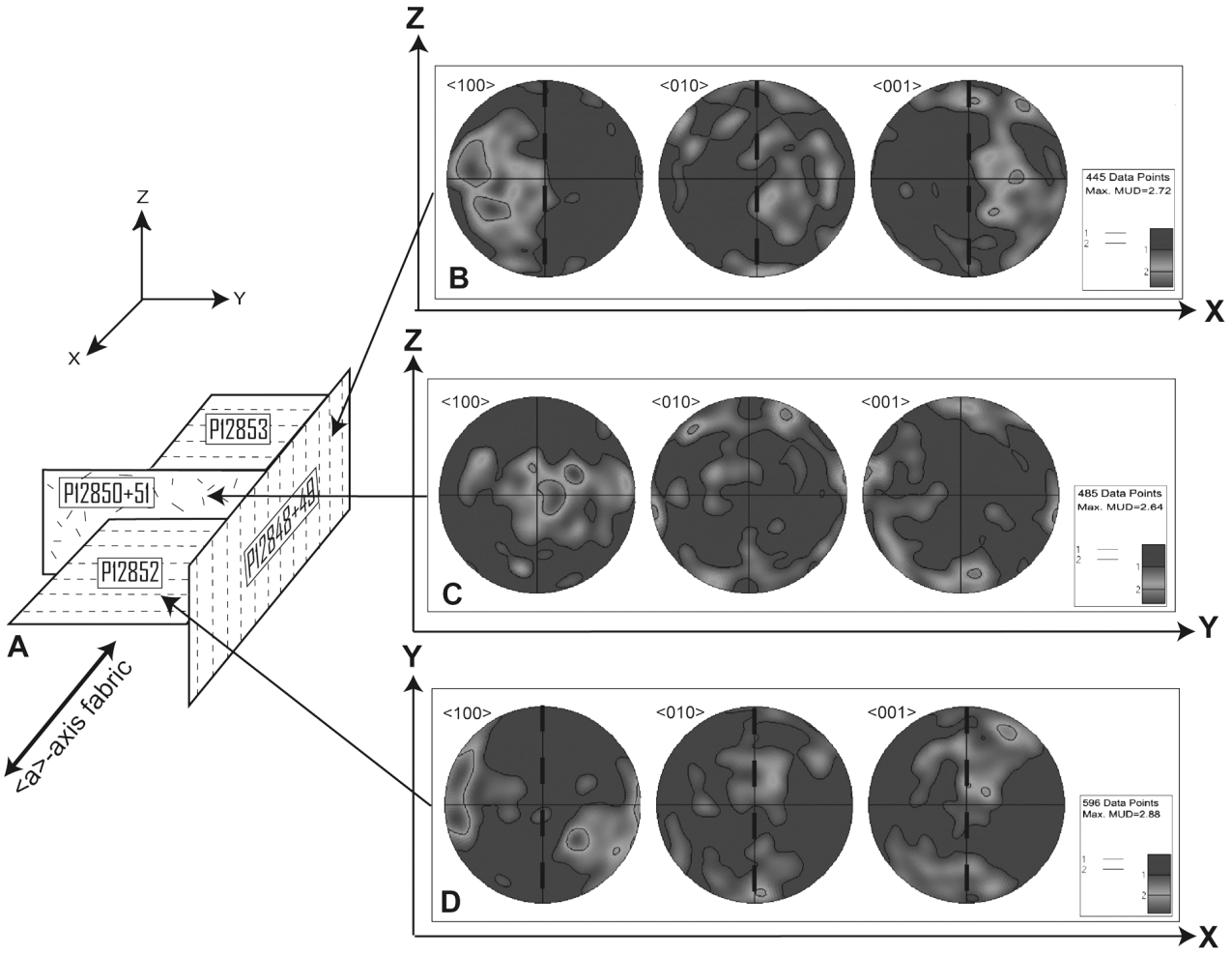

Fig. 5. A schematic sketch and equal area, lower hemisphere pole figures highlighting sample-scale, planar, short <a>-axis alignment fabric. a) A schematic sketch showing the orientation of samples and associated fabrics, determined using EBSD. b) A pole figure plot for section P12849. It highlights short <a>-axis alignment fabric; with the orientation of the long axes of the olivine crystals (i.e., the strike of the great circle containing the long axes—marked by black dashed line; <010> and <001> directions) running parallel to the Z-axis of the sample and the short axes (<a>-axes; <100> direction) plotting perpendicular to this. c) Pole figure plot for section P12850. Shows short <a>-axis alignment fabric in the plane of the section. Therefore short axes (<100> direction) cluster in the center of the pole figure and long axes (<010> and <001> directions) run around the perimeter of the pole figure. d) Pole figure plot for section P12852. Highlights short <a>-axis alignment fabric; with the long axes of the olivine crystals (black dashed line) running roughly parallel to the Y-axis of the sample and the short axes plotting perpendicular to this. Note: All pole figures are equal area, lower hemisphere projection. The three sections not shown in this figure are parallel to Figs. 5b–5d and therefore show the same fabric orientations.

representative fabric of a sample (Ismaïl and Mainprice 1998). Thus, typically 300–700 grains were analyzed and plotted for each area included in this study.

RESULTS

Analysis A: Fayalitic Olivine in Allende Matrix—Away from Inclusions

EBSD fabric analysis of fayalitic olivine was undertaken for multiple areas in Allende matrix in each of the six thick sections. The areas chosen for analysis were distal to chondrules and CAIs in order to reduce their influence on any fabric that might be present. For example, we have determined that a chondrule of 400 μm diameter influences the orientation of its surrounding matrix for ~200 μm. Therefore, where possible, areas chosen for analysis were at least 200 μm away from chondrules and CAIs in all directions. These sections contained no DIs. However, it should be noted that we are unaware of the presence of such components in the third dimension.

For each section, 3–6 areas of typically 60 × 60 μm were analyzed. A total of 25 areas were analyzed for all six sections. Each area consisted of 90,000 (300 × 300) raw data points and, once processed and filtered to one point per grain, contained ~500 individual grain analyses. Thus, this part of

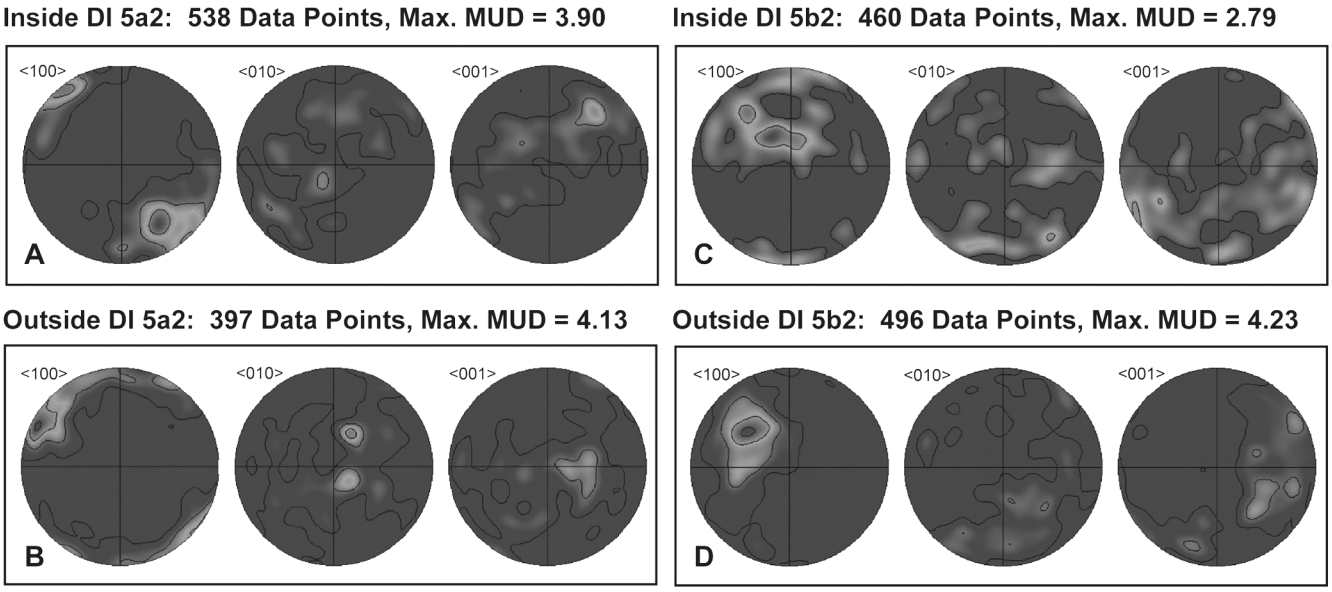

Fig. 6. Equal area, lower hemisphere pole figure plots for areas internal to and external to DIs. a) A pole figure plot for EBSD data obtained inside DI 5a2. b) A pole figure plot for EBSD data obtained outside of DI 5a2. Both (a) and (b) show the same short <a>-axis alignment fabric orientation. c) A pole figure plot for EBSD data obtained inside DI 5b2. d) A pole figure plot for EBSD data obtained outside of DI 5b21. Both (c) and (d) show the same short <a>-axis alignment fabric orientation.

the study draws on a total data set of ~12,500 individual grain analyses.

For all areas analyzed, there is a weak but consistent short <a>-axis alignment fabric, with an average maximum intensity of ~3 MUD (Fig. 5). The <a>-axis maximum has a consistent orientation in three dimensions (i.e., the fabrics measured from sections in different orientations can be rotated onto each other), which is aligned in the X-Y plane, roughly parallel to the X direction of the reference frame defined in Fig. 5. Individual platy olivine grains with a short <a>-axis crystal morphology appear to be stacked like tiles in a consistent, planar orientation, the plane being perpendicular to the preferred <a>-axis alignment. A consequence of this short-axis alignment fabric orientation is that planar fabrics can be observed in the matrix olivine grains in sections parallel to the X-Z and X-Y planes (Figs. 5b and 5d), illustrated by the orientation of the long axes (i.e., the strike of the great circle containing the long axes; <010> and <001> directions) being approximately parallel to the Z and Y planes, respectively. The grains appear randomly oriented in sections parallel to the Y-Z plane (Fig. 5c), indicated by the long axes being spread around the perimeter of their pole figures (<010> and <001>).

Analysis B: Fayalitic Olivine in Sections Containing DIs

In order to investigate the effect of DIs on the weak, planar fabric in the Allende host matrix, EBSD analysis of fayalitic olivine was conducted for several areas (typically 2–3 areas of 60 × 60 μm) in the Allende host matrix, in each of the five thin sections containing DIs. The areas chosen were as far away as possible from the DI to avoid detecting any DI rim fabric that might be present. These areas were also distal to chondrules and CAIs, again to reduce their influence on any fabric present. These results showed that the weak, planar fabric (average ~3 MUD max) in host Allende matrix in sections containing no DIs may be slightly strengthened (average ~4 MUD max) in the sections that do contain DIs.

Additionally, within each of the five sections containing DIs, EBSD analysis of fayalitic olivine was conducted inside each of the DIs. Typically, 1–2 areas of 60 × 60 μm were analyzed. This analysis revealed that, in all five sections, there is a fabric within dark inclusions that has the same orientation as the host Allende matrix fabric. This can be observed in Fig. 6, where the short <a>-axes (<100> direction) cluster in the same orientation internally (Figs. 6a and 6c) and externally (Figs. 6b and 6d) of the two DIs represented.

Analysis C: Fayalitic Olivine Adjacent to DIs

EBSD fabric analysis of fayalitic olivine was conducted for several matrix areas directly adjacent to DIs, for all five DIs. This analysis revealed that matrix directly adjacent to the DI becomes oriented around the margin of the DI (Fig. 7), with the long axes of the platy olivines (i.e., the strike of the great circle containing the long axes; <010> and <001> directions) being oriented parallel to the side of the DI and the short axes (<a>-axes; <100> direction) oriented

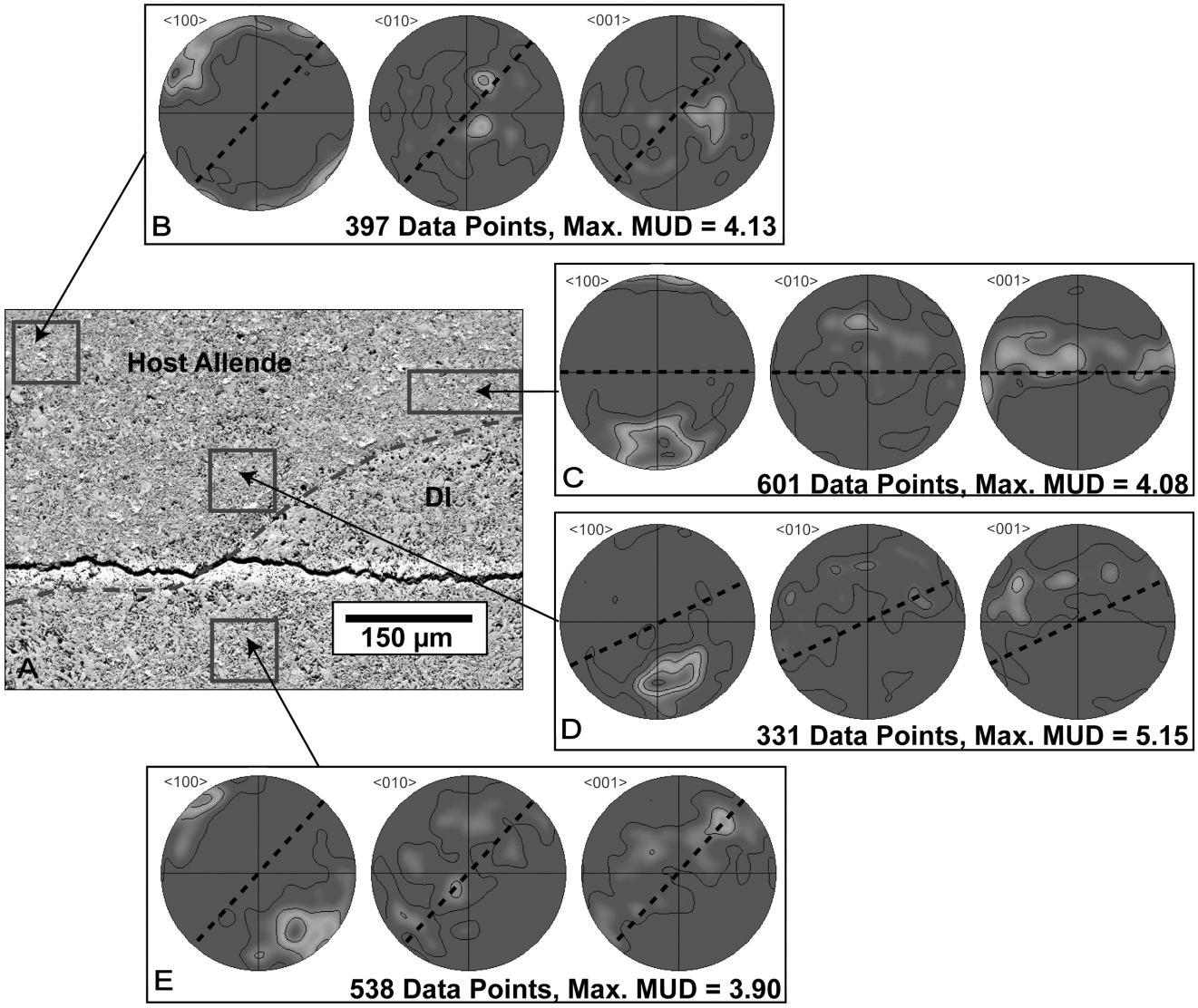

Fig. 7. EBSD analysis of Allende matrix directly adjacent to DI 5a2 and surrounding areas. a) An SEM, BSE image showing edge of DI (marked by the black dashed line). DI is observed below the line and Allende host matrix above. Areas outlined by black boxes indicate areas of EBSD analysis. b) and e) Equal area, lower hemisphere pole figure plot for areas outside and inside DI. It indicates short <a>-axis alignment fabric, with long axes of matrix olivines running from top right to bottom left of the sample (marked by black dashed line). Note: In addition to these areas, two more areas inside the DI and two more within the Allende host matrix were analyzed and show the same short <a>-axis alignment fabric orientation. c) and d) Equal area, lower hemisphere pole figure plots for areas directly adjacent to and above the DI margin. Shows spread of long axes (<010> and <001> directions) along a great circle, whose strike (marked by the black dashed line) is roughly parallel to the adjacent DI margin, with the <a>-axes (<100> direction) clustering perpendicular to this. Thus, indicating a short <a>-axis alignment fabric with the long axes of the matrix olivines being aligned roughly parallel to the margin of the DI, which is different to the fabric away from the DI margin (Figs. 7b and 7e).

perpendicular to this (Figs. 7c and 7d). Thus, a short <a>-axis alignment fabric is observed directly adjacent to the DI margin and its orientation is controlled by the shape of the DI. These fabric orientations, directly adjacent to the DI margin, tend to differ from the orientation of the planar, short <a>-axis alignment fabric within the DI and the host Allende matrix, distal to the DI (Figs. 7b and 7e). The exact thickness of the area directly adjacent to DI margins, in which fayalitic olivine becomes preferentially oriented, has not been determined. However, we estimate it to be >100 µm and <300 µm.

It is worth noting that this local orientation of host Allende matrix directly adjacent to DIs is not consistent around the entire perimeter of DIs (Fig. 8). Some locations directly adjacent to the DI do not become oriented against the margin of the DI, as indicated in Fig. 8e, with no parallel orientation of the long axes of the crystals (<010> and <001> directions) and the DI margin.

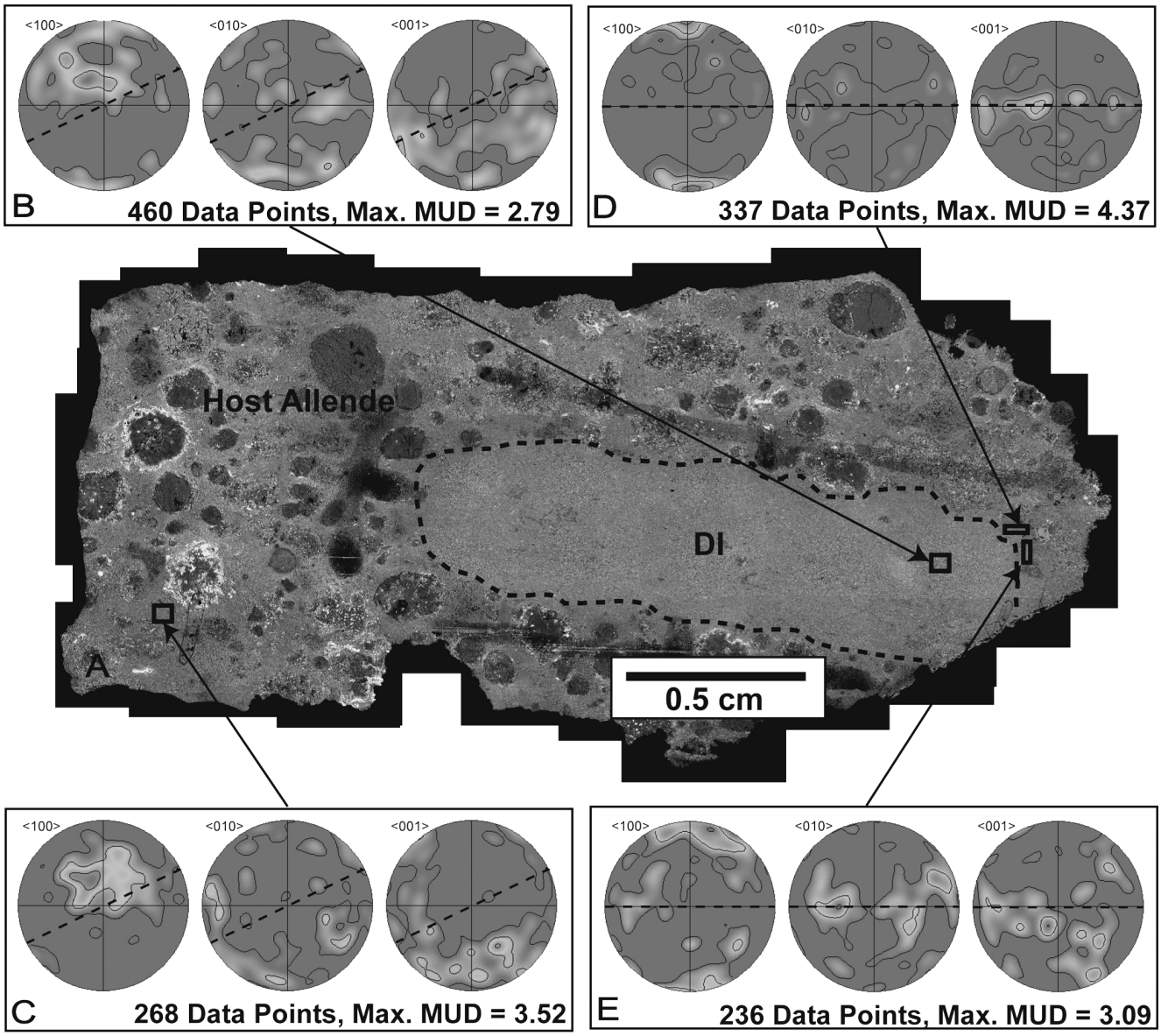

Fig. 8. EBSD analysis of Allende matrix directly adjacent to DI 5b2 and surrounding areas. a) An SEM, BSE image showing edge of DI (marked by the black dashed line). Areas outlined by black boxes indicate areas of EBSD analysis. b) and c) Equal area, lower hemisphere pole figure plot for areas inside and outside DI. It indicates short <a>-axis alignment fabric, with long axes of matrix olivines running from approximately the top right to bottom left of the sample (marked by the black dashed line). d) and e) Equal area, lower hemisphere pole figure plots for areas directly adjacent DI margin. Shows short <a>-axis alignment fabric, with long axes of matrix olivines running from left to right of the sample (marked by black dashed line). Thus, indicating a short <a>-axis alignment fabric with the long axes of the matrix olivines not being aligned parallel to the margin of the DI.

Analysis D: Fayalitic Olivine Directly Adjacent to CAIs

Several matrix areas were analyzed around the margins of two CAIs in sections not containing DIs. While this did indicate the presence of a short <a>-axis alignment fabric parallel with the margins of the CAIs (Fig. 9), this is often weaker than is observed adjacent to DIs (average ~4 MUD max), with an average maximum intensity ~2.8 MUD (Fig. 9), and is often poorly defined.

DISCUSSION

The presence of a weak, broadscale, short <a>-axis alignment fabric in Allende matrix away from inclusions would suggest that the parent asteroid has undergone a deformational shortening event, locally or regionally, causing a rotation of the platy grains to produce a uniform, planar fabric. Many previous textural studies of chondrites, including several other carbonaceous chondrites, using

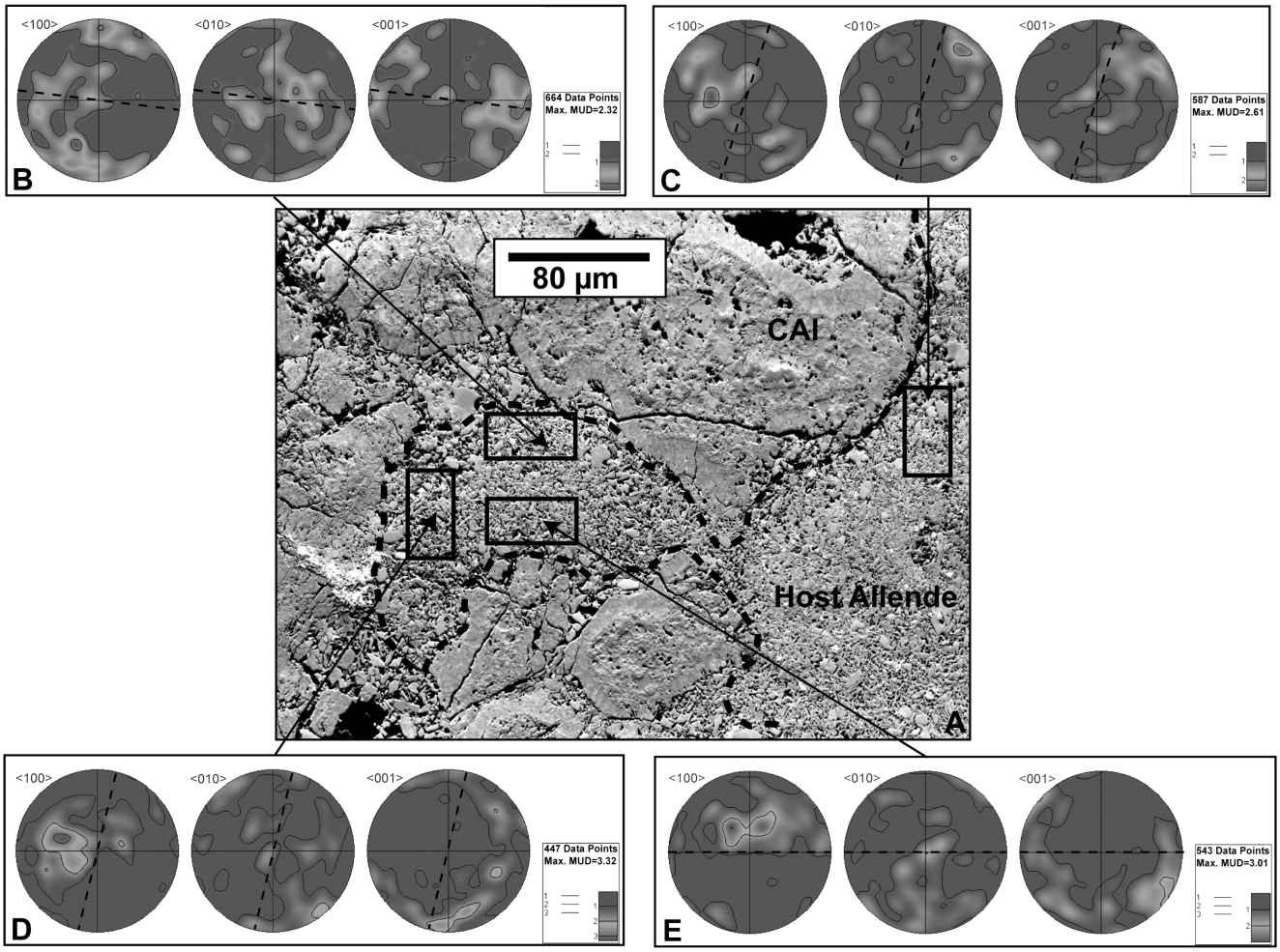

Fig. 9. a) An SEM, BSE image showing the approximate margin of CAI (marked by the black dashed line) and areas of EBSD analyses in Allende matrix, adjacent to the CAI margin (outlined by black boxes). b), d), and e) Equal area, lower hemisphere pole figure plots of the areas adjacent to the CAI margin. All pole figures show a spread of the long axes (<010> and <001> directions) along a great circle, whose strikes (the black dashed lines) are roughly parallel to the adjacent CAI margin, with the <a>-axes (<100> direction) clustering perpendicular to this. These data reveal a short <a>-axis alignment fabric becoming oriented around the CAI margin, but it is weak (average ~2.8 MUD max) and often poorly defined.

macroscale analytical techniques or qualitative observations, have highlighted the presence of pervasive planar fabrics (e.g., Sneyd et al. 1988; Martin and Mills 1980; Fujimura et al. 1983; Bunch and Chang 1980; Keller and Thomas 1991; Cain et al. 1986; Zolensky et al. 1997; Bérczi et al. 2002), all of which have been attributed to compaction-induced deformational shortening on the meteorite parent body. Possible driving forces for such compactions include static gravitational burial compaction on a parent body of ~100 km or more in diameter (Fujimura et al. 1983) or dynamic impact-induced deformations. Both would result in the compaction of matrix, rotation of grains, and a reduction in porosity. Sneyd et al. (1988) proposed that the degree of deformation, in ordinary chondrites, correlates with shock intensity, and therefore concluded that impact events were responsible for the planar fabric observed. Fujimura et al. (1983) used the degree of rotation of phyllosilicates, subparallel to the plane of deformation, in Murchison (a type 2 carbonaceous chondrite) to quantify the total strain. They calculate that an axial strain of only 8.7% is required to explain the preferred orientation observed, arguing that this is one of the weakest cases ever reported, implying that the mechanical processes experienced were weak in intensity and therefore unlikely to be impact induced.

Studies of Allende have thus far revealed no evidence of shock processes affecting this meteorite. This may suggest that the fabric we observe was formed by a less dynamic process, such as gravitational compaction, or that the Allende meteorite samples a deep level in the asteroid where the effect of impact was less intense.

It has been proposed that Allende experienced hydration followed by dehydration on its parent asteroid (e.g., Krot et al.

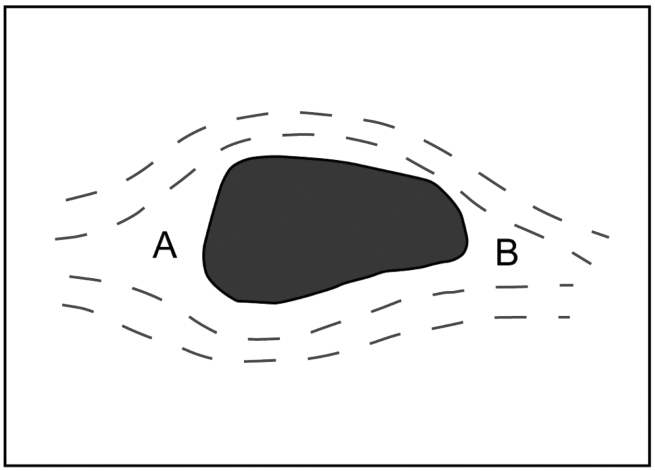

Fig. 10. A schematic diagram illustrating possible augen-like fabric around the margin of DIs. A and B represent strain shadow areas, where the short <a>-axis alignment fabric that is oriented around the margin of the DI is not observed.

1995). It should be noted that alone, such processes cannot generate a fabric such as the one we observe. Indeed, the most likely effect of hydration and dehydration would be to destroy any preexisting fabric. Further discussion of the origin of the fabric observed in Allende is beyond the scope of this study.

The modest increase in fabric intensity in Allende matrix in sections containing DIs may be the result of reworking of the matrix surrounding DIs during their emplacement into their current position in the Allende host. Alternatively, it may have been caused by deformation partitioning between the DI and surrounding matrix. If the inclusion acted more rigidly than the surrounding matrix during a deformation event, then the surrounding matrix would have had to absorb more strain, thus intensifying the deformation close to the inclusion. However, the spatial relationship between the five sections containing DIs and the six sections not containing DIs is unknown. It is possible that variations in matrix fabric intensity occur throughout the asteroid; the apparent increase in fabric intensity in sections containing DIs may reflect this.

The presence of a fabric inside DIs with the same orientation as the fabric external to DIs suggests that this fabric has been imposed after DIs were incorporated into their present position, ruling out reworking as the cause of the increased fabric intensity in sections containing DIs. These data also imply that DIs were incorporated at an early stage in the history of the Allende parent body (i.e., before the parent body was lithified and had a chance for deformational fabrics to develop), arguing against the idea that DIs are fragments from another lithified part of the asteroid (Kojima and Tomeoka 1996; Fruland et al. 1978). If they were in fact fragments from another lithified part of the asteroid, we would not expect them to preserve the same fabric orientation as the material that surrounds them. In addition, both DIs and Allende matrix are highly porous (~25%) (Corrigan et al. 1997), and it is probable that their porosities were significantly greater prior to the deformational shortening, responsible for the fabrics we observe. Mobilizing a highly porous DI during an impact brecciation event without imposing a fabric and incorporating it into a highly porous matrix while maintaining high porosities in all of the affected materials is improbable. Instead, it is likely that DIs accreted at the same time as the Allende matrix material and experienced the same mild compactional events.

The occurrence of short-axis alignment fabrics becoming oriented with the margins of DIs and CAIs, indicates that these components were in situ during deformation of the asteroid, causing the surround matrix to rotate and orient around them. The absence of a consistent fabric around the entire perimeter of DIs indicates that this fabric is likely to be related to the same deformational shortening event that is responsible for the formation of the other planar fabrics observed and has caused strain shadows to develop around parts of the inclusions' margins, analogous to augen in terrestrial rocks (Fig. 10).

The cause of the weakened fabric around the margin of CAIs is unknown. It is possible that this is related to their very irregular morphology, which will prevent the formation of a strong fabric around their margins. However, the CAIs studied are in the sections not containing DIs, where the general matrix fabric intensity is somewhat weaker than in the sections containing DIs. Thus, this apparently weakened fabric around the margin of CAIs may be an effect of local variations in fabric intensity on the asteroid. It is not possible to determine whether CAIs also have strain shadow areas around their perimeter, due to their irregular nature.

Finally, the presence of a well-developed chondrule rim fabric around the entire perimeter of chondrules in Allende, as determined by Bland et al. (2003) and P. A. Bland (personal communication, 2003), implies that this was not produced by the same deformational shortening event that generated the other planar fabrics we have observed. One possibility is that chondrule rim fabrics formed prior to their incorporation into the Allende host.

The origin of fayalitic olivine in the matrices of carbonaceous chondrites is a subject of continuing debate. Several authors have argued that morphologies (MacPherson et al. 1985) and chemistry (Kornacki and Wood 1984) of FeO-rich olivine in the matrices of CV3s are consistent with a formation by condensation from the solar nebula. However, the formation of fayalitic olivine in an equilibrium condensation model is complicated and requires higher than solar oxygen fugacities (Weinbruch et al. 1990). This led other researchers to explore a secondary origin for fayalitic olivine, with Krot et al. (1995, 1997) and Kojima and Tomeoka (1996) suggesting a formation through hydration and dehydration processes on the parent asteroid. Our data indicate that compressional forces acting on the parent body have produced a rotation of platy fayalitic olivine grains to

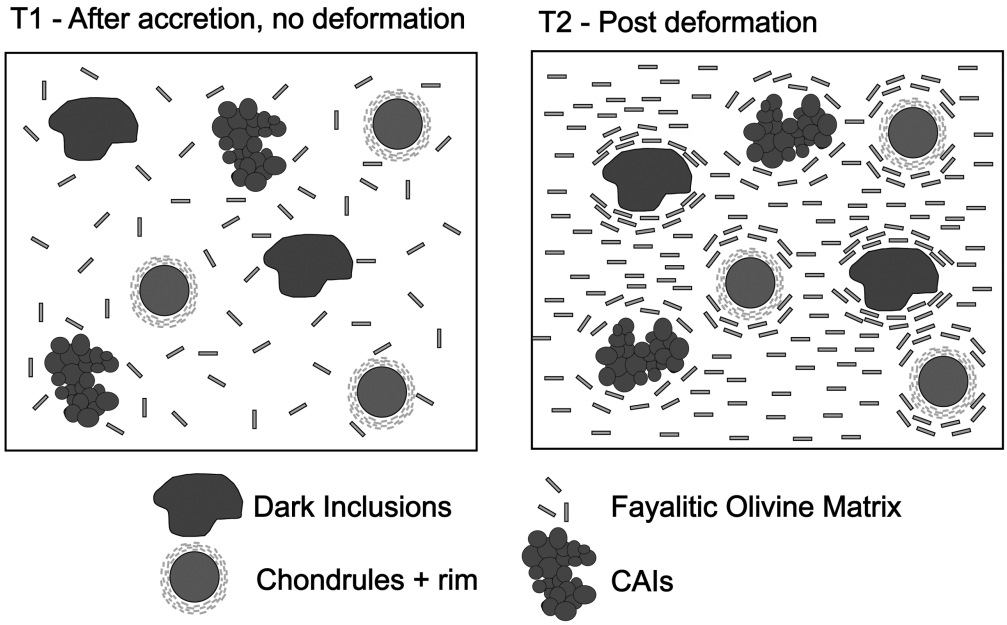

Fig. 11. A schematic diagram showing the orientation of fayalitic olivine in Allende matrix and its relationship to the larger components, both before and after deformation.

form short-axis alignment fabrics. This suggests that fayalitic olivine existed prior to the formation of such fabrics. This permits three possibilities for the formation of the fayalitic olivine:

1. Matrix and DIs accreted with a fayalitic component, requiring either fayalitic olivine condensation in the nebula or the formation of phyllosilicate (Ciesla et al. 2003) followed by dehydration in the nebula.
2. Hydration/dehydration on the asteroid was responsible for the formation of fayalitic olivine. But this must have occurred very early in the history of the parent asteroid, before any compressional forces had time to act. In this scenario, it would be preferable to find a formation mechanism for DIs that did not involve impact brecciation.
3. Fayalitic olivine in DIs and matrix is a pseudomorph. Lath-shaped grains with a different mineralogy, possibly forsteritic olivine or low-Ca pyroxene (Krot et al. 1997), were rotated during deformation, hydration produced phyllosilicates that pseudomorphed the primary phase, and phyllosilicates were dehydrated to fayalite, which retained the primary crystallographic orientation.

CONCLUSIONS

- EBSD analysis of the fayalitic olivine fraction of Allende matrix has highlighted a variety of different features:
  1. The presence of a weak, broad-scale, planar, short <a>-axis alignment fabric in the general Allende matrix, away from inclusions, which becomes intensified in proximity to DIs.
  2. DIs possess a short <a>-axis alignment fabric that is conformable with the broad-scale host Allende fabric.
  3. The occurrence of short <a>-axis alignment fabrics parallel with the margins of DIs and CAIs, although this appears to be less well-defined around the margins of CAIs and is not consistent around the entire perimeter of DIs.
  4. The presence of a well-developed, short <a>-axis chondrule rim fabric which rotates around the entire perimeter of chondrules (Bland et al. 2003; P. A. Bland, personal communication, 2003).
- It seems evident that the weak, broad-scale planar fabric was caused by deformational shortening events, either impact or gravitational compaction. However, the exact source cannot be determined from this work.
- The occurrence of a fabric inside DIs with the same orientation as the general host Allende matrix fabric, coupled with the development of local short <a>-axis alignment fabrics parallel with the margins of DIs and CAIs, would suggest that these components were in situ when the deformation, which was responsible for the weak, broad-scale planar fabric, occurred on the asteroid.
- The interaction between this weak, broadscale, planar fabric with the larger, more rigid clasts led to the development of locally intensified and orientated matrix fabrics and the development of strain shadows (Fig. 11).
- These observations provide a strong argument against DIs being lithic fragments from another part of the asteroid, mixed with the Allende host during impact

brecciation (Kojima and Tomeoka 1996; Fruland et al. 1978). Instead it seems likely that Allende DIs, CAIs, and matrix accreted at the same time and experienced the same deformational events.

- The presence of a well-developed, short-axis, chondrule rim fabric around the entire perimeter of chondrules in Allende (Bland et al. 2003; P. A. Bland, personal communication, 2003), implies that this was not produced by the same deformational event that generated the other planar fabrics we observed. One possibility is that chondrule rim fabrics formed prior to their incorporation into the Allende host (Fig. 11).
- Finally, our data indicate that compressional forces acting on the parent body have produced a rotation of platy fayalitic olivine grains to form short-axis alignment fabrics. The simplest interpretation is that fayalitic olivine existed prior to the formation of such fabrics. If hydration/dehydration on the asteroid was responsible for the formation of fayalitic olivine (Kojima and Tomeoka 1996; Krot et al. 1995, 1997), then alteration occurred early in the history of the parent asteroid, before any compressional forces had time to act (and we require a different origin for the incorporation of DIs than impact brecciation). Alternatively, fayalitic olivine formed later, and has perfectly pseudomorphed lath-shaped precursor minerals, allowing an earlier fabric to survive. We have found no evidence to suggest this, and furthermore, this explanation is rather convoluted. Taking our data at face value, the suggestion is that fayalitic olivine existed in matrix and DIs at the time that these components accreted.

Acknowledgments–This study was funded by Imperial College London. P. A. B. would like to thank the Royal Society for their support. The CamScan X500 was funded by HEFCE through the grant JR98LIPR. L. J. Chizmadia, M. E. Zolensky, and E. R. D. Scott provided reviews that greatly improved this manuscript. This is IARC (Impact and Astromaterials Research Centre) publication 2005-0723.

Editorial Handling—Dr. Edward Scott

REFERENCES

Bérczi Sz., Gál-Sólymos K., Kubovics I., and Puskás Z. Layered texture of Kaba CV3 chondrite (abstract). *Meteoritics & Planetary Science* 37:A16.

Bestmann M. and Prior D. J. 2003. Intragranular dynamic recrystallization in naturally deformed calcite marble: Diffusion accommodated grain boundary sliding as a result of subgrain rotation recrystallization. *Journal of Structural Geology* 25: 1597–1613.

Bland P. A., Prior D. J., and Hough R. M. 2003. A rock fabric in chondrite matrix (abstract). *Meteoritics & Planetary Science* 38: A100.

Brearley A. J. and Jones R. H. 1998. Chondritic meteorites. In *Planetary materials,* edited by Papike J. J. Washington D.C.: Mineralogical Society of America. pp. 3-1–3-307.

Bunch T. E. and Chang S. 1980. Carbonaceous chondrites II—Carbonaceous chondrite phyllosilicates and light element geochemistry as indicators of parent body processes and surface conditions. *Geochimica et Cosmochimica Acta* 44:1543–1577.

Cain P. M., McSween H. Y., Jr., and Woodward N. B. 1986. Structural deformation of the Leoville chondrite. *Earth and Planetary Science Letters* 77:165–175.

Ciesla F. J., Lauretta D. S., Cohen B. A., and Hood L. L. 2003. A nebular origin for chondritic fine-grained phyllosilicate. *Science* 299:549–552.

Corrigan C. M., Zolensky M. E., Dahl J., Long M., Weir J., Sapp C., and Burkett P. J. 1997. The porosity and permeability of chondritic meteorites and interplanetary dust particles. *Meteoritics & Planetary Science* 32:509–515.

Fruland R. M., King E. A., and McKay D. S. 1978. Allende dark inclusions. Proceedings, 9th Lunar and Planetary Science Conference. pp. 1305–1329.

Fujimura A., Kato M., and Kamazawa M. 1983. Preferred orientation of phyllosilicate (001) in matrix of Murchison meteorite and possible mechanisms of generating the oriented texture in chondrites. *Earth and Planetary Science Letters* 66:25–32.

Ismaïl W. B. and Mainprice D. 1998. An olivine fabric database: An overview of upper mantle fabrics and seismic anisotropy. *Tectonophysics* 296:145–157.

Keller L. P. and Thomas K. L. 1991. Matrix mineralogy of the Bali CV3 carbonaceous chondrite (abstract). 22nd Lunar and Planetary Science Conference. p. 705.

Kojima T. and Tomeoka K. 1996. Indicators of aqueous alteration and thermal metamorphism on the CV parent body: Microtextures of a dark inclusion from Allende. *Geochimica et Cosmochimica Acta* 60:2651–2666.

Kornacki A. S. and Wood J. A. 1984. The mineral chemistry and origin of inclusion matrix and meteorite matrix in the Allende CV3 chondrite. *Geochimica et Cosmochimica Acta* 48:1663–1676.

Krot A. N., Scott E. R. D., and Zolensky M. E. 1995. Mineralogical and chemical modification of components in CV3 chondrites: Nebular or asteroidal processing? *Meteoritics* 30:748–775.

Krot A. N., Scott E. R. D., and Zolensky M. E. 1997. Origin of fayalitic olivine rims and lath-shaped matrix olivine in the CV3 chondrite Allende and its dark inclusions. *Meteoritics* 32:31–49.

MacPherson G. J., Hashimoto A., and Grossman L. 1985. Accretionary rims on inclusions in the Allende meteorite. *Geochimica et Cosmochimica Acta* 49:2267–2279.

Martin P. M. and Mills A. A. 1980. Preferred orientations in meteorites. *Earth and Planetary Science Letters* 51:18–25.

Morden S. J. and Collinson D. W. 1992. The implications of the magnetism of ordinary chondrite meteorites. *Earth and Planetary Science Letters* 109:185–204.

Peck J. A. 1984. Origin of the variation in properties of CV3 meteorite matrix and matrix clasts (abstract). 15th Lunar and Planetary Science Conference. pp. 635–636.

Prior D. J., Boyle A. P., Brenker F., Cheadle M. C., Day A., Lopez G., Peruzzo L., Potts G. J., Reddy S., Spiess R., Timms N. E., Trimby P., Wheeler J., and Zetterström L. 1999. The application of electron backscatter diffraction and orientation contrast imaging in the SEM to textural problems in rocks. *American Mineralogist* 84:1741–1759.

Scott E. R. D., Barber D. J., Alexander C. M. O'D., Hutchison R., and Peck J. A. 1988. Primitive material surviving in chondrites: Matrix. In *Meteorites and the early solar system,* edited by Kerridge J. F. and Matthews M. S. Tucson, Arizona: The University of Arizona Press. pp. 718–745.

Scott E. R. D. and Krot A. N. 2003. Chondrites and their components. In *Meteorites, comets, and planets,* edited by Davis A. M. Oxford: Elsevier Press. pp. 143–200.

Sneyd D. S., McSween H. Y. Jr., Sugiura N., Strangway D. W., and Nord G. L. Jr. 1988. Origin of petrofabrics and magnetic anisotropy in ordinary chondrites. *Meteoritics* 23:139–149.

Tomeoka K., Yamahana Y., and Sekine T. 1999. Experimental shock metamorphism of the Murchison CM carbonaceous chondrite. *Geochimica et Cosmochimica Acta* 63:3683–3703.

Weinbruch S., Palme H., Müller W. F., and Goresy A. E. 1990. FeO-rich rims and veins in Allende forsterite: Evidence for high temperature condensation at oxidizing conditions. *Meteoritics* 25:115–125.

Weisberg M. K. and Prinz M. 1998. Fayalitic olivine in CV3 chondrite matrix and dark inclusions: A nebular origin. *Meteoritics & Planetary Science* 33:1087–1099.

Zolensky M. E., Mittlefehldt D. W., Lipschutz M. E., Wang M. S., Clayton R. N., Mayeda T. K., Grady M. M., Pillinger C., and Barber D. 1997. CM chondrites exhibit the complete petrologic range from type 2 to 1. *Geochimica et Cosmochimica Acta* 61: 5099–5115.